processes

MDPI

Article

Study on the Conveying Characteristics of a Hanged Harvester Vibrating Screen for Ligusticum Chuanxiong

Jiarui Wang [1,2], Min Liao [1,2,*], Hailong Xia [1,2], Rui Chen [1,2], Junju Li [1,2] and Yajun Yang [1,2]

[1] Institute of Modern Agricultural Equipment, Xihua University, Chengdu 610039, China
[2] School of Mechanical Engineering, Xihua University, Chengdu 610039, China
* Correspondence: liaomin@mail.xhu.edu.cn

Abstract: The problem of soil and Chuanxiong tuber congestion on vibrating screens usually exists during the Chuanxiong mechanized harvesting process. To address this problem, the conveyance performance of a crankshaft rocker vibrating screen was studied. By establishing and solving the dynamics and kinematics equations for the crankshaft rocker vibrating mechanism and Chuanxiong soil residue, the acceleration of the vibrating screen and Chuanxiong-soil residue was studied. The sliding speed, motion process, and conveying distance of the Chuanxiong soil residue were also analyzed. The theoretical analysis results indicated that the acceleration of the vibrating screen depends on the rod lengths of the vibrating mechanism and the crank rotational speed and position. The displacement of the Chuanxiong-soil residue along the positive sliding direction in a cycle was more significant than that of the negative sliding direction. The appropriate advancement speed of the harvester was also obtained. The RecurDyn and EDEM coupling simulation was conducted. The simulation results verified the theoretical analysis. In the simulation, the Chuanxiong-soil residue was effectively conveyed. The field tests were conducted to verify the theoretical analysis. The harvester was tested in the field with crank rotational speeds of 0 r/min, 120 r/min, and 240 r/min, and advancement speeds of 0.5 m/s, 1 m/s, 1.5 m/s, and 2 m/s. The results showed that there was no congestion in the screen during the working process when the rotational speed of the crank was 240 r/min, and the advancement speed of the harvester was no faster than 1.5 m/s. When the crank rotational speed was 240 r/min, and the advancement speeds were 0.5 m/s, 1 m/s, and 1.5 m/s, the weights of Chuanxiong and soil on the screen after the test were 71.5 kg, 84.7 kg, and 105.7 kg, respectively. The field tests verified the conveyance performance of the vibrating screen. This study can provide a theoretical reference for designing the crankshaft rocker vibrating mechanism for the rhizome harvesting machine.

Keywords: Chuanxiong harvester; vibrating screen; kinematic analysis; conveying characteristics

Citation: Wang, J.; Liao, M.; Xia, H.; Chen, R.; Li, J.; Yang, Y. Study on the Conveying Characteristics of a Hanged Harvester Vibrating Screen for Ligusticum Chuanxiong. *Processes* **2024**, *12*, 1323. https://doi.org/10.3390/pr12071323

Academic Editor: Dariusz Dziki

Received: 20 May 2024
Revised: 23 June 2024
Accepted: 24 June 2024
Published: 26 June 2024

1. Introduction

Ligusticum Chuanxiong is a traditional Chinese herb that can not only be used as an ingredient in soup but also as a medicinal herb [1,2]. During the harvest process, the mixture of Chuanxiong tuber and soil often becomes clogged in the Chuanxiong harvester. In this study, the mixture of Chuanxiong tubers and soil on the vibrating screen is abbreviated as Chuanxiong-soil residue. The Chuanxiong harvester must ensure a smooth conveyance of the Chuanxiong-soil residue on the vibrating screen. Studying the movement pattern of the Chuanxiong-soil residue on the screen is crucial for analyzing the conveyance efficiency of the vibrating screen. Solving the blockage problem of Chuanxiong-soil residue will facilitate the normal operation of the harvester and improve harvesting efficiency.

Screens are widely used to separate and transport materials [3,4]. In the agricultural machinery industry, screens are commonly used in harvesting devices [5] and cleaning devices [6]. In the study of harvesting devices, researchers always analyze the separating performance [7,8], net harvesting performance [9], or loss rate of the vibrating screen [10,11].

However, the particle conveyance ability is also very important and rarely studied. This capacity directly affects the congestion of the harvester during the operation process. Thus, it is necessary to analyze the conveyance ability of the designed Chuanxiong harvester vibrating screen. Previous studies have analyzed the conveyance of the screen by conducting the analysis on particle force and particle motion process [12,13]. In the aspect of analyzing particle forces on screens, the previous study found that the non-linear forces on the residue in the direction of the screen surface mainly include inertial forces and sliding friction [14]. The friction coefficients and excitation forces have a significant influence on the velocity of residues on the screen, which directly influence the motion laws of materials on the screens [15]. In the aspect of motion analysis, researchers constructed mathematical analysis models, and some researchers derived velocity curves by analyzing the acceleration of the vibrating screen [16,17]. Han et al. [18] analyzed the movement of a part on the vibrating track of the bowl feeder during the conveying process. Ma et al. [19] found that the rotation angle of the front swing bar has a positive influence on the backward movement rate of particles. Song et al. [20] studied the motion trajectory to determine the optimal speed range for particle mixing and transportation. Yang et al. [21] studied the forces, stratification mechanisms, and throwing principles of materials on the screen. The materials on the screen can be conveyed by sliding or jumping motion [22]. Zhou et al. [23] conducted a study to analyze the motion state of the materials with the help of high-speed cameras.

During the harvesting process of Chuanxiong, the Chuanxiong-soil residue frequently clogs on the sieve, posing a challenging issue. Although the above researchers studied the motion process of particles on screens, the theoretical analysis of the time corresponding to the motion process of Chuanxiong-soil residue on screens was rarely studied. The existing studies mainly conducted mechanical analysis on the motion state of material on screen, without quantitative analysis of the motion characteristics corresponding to the motion state. However, researchers seldom conducted theoretical analyses that combined kinematic parameters such as the velocity and acceleration of residues on the screens. In this study, the motion process of Chuanxiong-soil residue on the screen was studied according to the kinematics and kinetics principles. Then, a suitable advancement speed was obtained for the harvester to convey the Chuanxiong-soil residue backward effectively. The relative motion process between the Chuanxiong-soil residues and the vibrating screen was studied more deeply. Then, the conveying process of the Chuanxiong-soil residue on the vibrating screen was analyzed by using the coupling simulation of EDEM2020 and RecurDynV9R4. Finally, motion law tests were conducted to verify the theoretical analysis of the vibrating screen using an accelerometer. The field tests were conducted to verify the actual Chuanxiong-soil residue conveying performance of the vibrating screen.

2. Structural Composition and Working Principle of the Crankshaft Rocker Vibrating Mechanism

The Chuanxiong harvester and a typical Chuanxiong tuber are shown in Figure 1. The Chuanxiong harvester is hanged on a tractor (as shown in Figure 1a) and can excavate the Chuanxiong tubers under the soil. Chuanxiong tubers are approximately spherical, but they have an irregular surface and are always covered with a lot of soil (as shown in Figure 1b).

The schematic diagram of the Chuanxiong harvester and the working principle of the crankshaft rocker vibrating screen are shown in Figure 2. The overall structure of the Chuanxiong harvester is shown in Figure 2a. The crankshaft rocker vibrating screen is mainly composed of the crankshaft rocker vibrating mechanism, a vibrating side plate, and a vibrating screen. The simplified working sketch of the vibrating mechanism is shown in Figure 2b. The crankshaft rocker vibrating mechanism consists of a crank, driving link, driven rocker1, fixed link, and driven rocker2. The two driven rockers have identical lengths. The vibrating screen is made of parallel steel bars and connected to vibrating side plates. The vibrating side plates are hinged with driven rockers. The angle between

the vibrating screen and the horizontal surface is the screen surface tilting angle α. The parameters of the crankshaft rocker vibrating mechanism are shown in Table 1. In the working process, the vibrating mechanism is driven by the crank. The drive link rod causes the vibrating screen to reciprocate vibration, facilitating the transmission of the Chuanxiong-soil residues, preventing congestion on the screen, and enabling continuous harvesting operation. The motion sketch of the vibrating mechanism is simplified, as shown in Figure 2c. The crank rotates clockwise during the working process, and the crank rotation center O is the origin of the Cartesian orthogonal coordinate system. The positive direction of the x-axis is horizontal to the left. The positive direction of the y-axis is vertical downward. The OA, AB, and BC rods represent the crank, the drive link rod, and the driven rocker, respectively. The angles of the OA, AB, and BC rods with the x-axis are φ_1, φ_2, and φ_3, and the lengths are L_1, L_2, and L_3, respectively. The length of the OC rod is L_4.

Figure 1. Chuanxiong harvester and a typical Chuanxiong tuber. (**a**) Chuanxiong harvester. (**b**) Chuanxiong tuber.

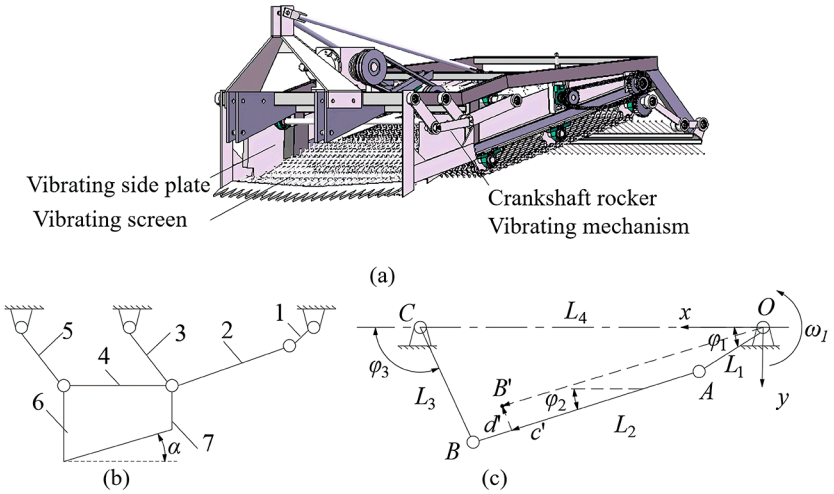

Figure 2. Crankshaft rocker vibrating screen. (**a**) Overall structure of the Chuanxiong harvester. (**b**) Simplified working sketch of the crankshaft rocker vibrating mechanism: 1—Crank, 2—Driving link, 3—Driven rocker1; 4—Fixed link; 5—Driven rocker 2; 6—Vibrating side plate; 7—Vibrating screen. (**c**) Motion sketch of vibrating mechanism.

Table 1. Parameters of the crankshaft rocker vibrating mechanism.

Parameter Name	Value
Crank radius L_1 (mm)	50
Driving link length L_2 (mm)	410
Driven rocker 1/2 length L_3 (mm)	200
Fixed link length L_4 (mm)	270
Screen surface tilting angle α (°)	20
Crank rotational speed n (r/min)	240

3. Theoretical Analysis of Screen and Chuanxiong-Soil Residue

3.1. Acceleration Analysis of Vibrating Screen

The motion law of a vibrating screen is the same as that of the hinged point B on the crankshaft rocker vibrating mechanism. Supposing the position vectors of any point B' on the driving link rod are c' and d', the absolute position vector of point B' in the coordinate system is $l_{B'} = \overrightarrow{OB'}$ [24], and the vector Equation (1) is:

$$\vec{l}_{B'} = \vec{L}_1 + \vec{c'} + \vec{d'} \tag{1}$$

The complex vector form of Equation (1) is Equation (2):

$$\vec{L}_{B'} = L_1 e^{i\varphi_1} + c' e^{i\varphi_2} + d' e^{i(\varphi_2 + 90^o)} \tag{2}$$

Equation (2) is simplified according to Euler's formula. Then, the second derivative is found for time t, and the acceleration of point B' in the x-axis and y-axis direction ($a_{B'x}$ and $a_{B'y}$) can be obtained through Equation (3):

$$\begin{cases} a_{B'x} = -\left[\omega_1^2 L_1 \cos\varphi_1 + a_2(c' \sin\varphi_2 + d' \cos\varphi_2)\right] + \omega_2^2(c' \cos\varphi_2 - d' \sin\varphi_2) \\ a_{B'y} = -\omega_1^2 L_1 \sin\varphi_1 + a_2(c' \cos\varphi_2 - d' \sin\varphi_2) - \omega_2^2(c' \sin\varphi_2 + d' \cos\varphi_2) \\ \omega_1 = \frac{2\pi n}{60} \end{cases} \tag{3}$$

where ω_1 is the angular velocity of the OA rod, rad/min; ω_2 is the angular velocity of the AB rod, r/min; a_2 is the angular acceleration of the AB rod, m/s^2.

Substituting $c' = L_2$ and $d' = 0$ into Equation (3) to obtain the acceleration of point B in the x-axis and y-axis direction (a_{Bx} and a_{By}), Equation (4) can be obtained as:

$$\begin{cases} a_{Bx} = -\omega_1^2 L_1 \cos\varphi_1 + L_2 a_2 \sin\varphi_2 + L_2 \omega_2^2 \cos\varphi_2 \\ a_{By} = -\omega_1^2 L_1 \sin\varphi_1 + L_2 a_2 \cos\varphi_2 - L_2 \omega_2^2 \sin\varphi_2 \end{cases} \tag{4}$$

By using the closed vector analytical method to analyze the motion of the vibrating mechanism, the angular acceleration of the AB rod a_2 can be obtained through Equation (5):

$$a_2 = \frac{\theta L_3 \cos\varphi_3 - \mu L_3 \sin\varphi_3}{L_2 L_3 \sin\varphi_2 \cos\varphi_3 - L_2 L_3 \cos\varphi_2 \sin\varphi_3} \tag{5}$$

where θ and μ can be obtained by Equation (6):

$$\begin{cases} \theta = \omega_1^2 L_1 \cos\varphi_1 - \omega_1^2 L_2 \cos\varphi_2 - \omega_3^2 L_3 \cos\varphi_3 \\ \mu = -\omega_1^2 L_1 \sin\varphi_1 - \omega_1^2 L_2 \sin\varphi_2 + \omega_3^2 L_3 \sin\varphi_3 \end{cases} \tag{6}$$

where the angle φ_2 between the AB rod and the x-axis and the φ_3 between the BC rod and the x-axis can be obtained through Equation (7):

$$\begin{cases} \varphi_2 = \arcsin\frac{\varepsilon^2 + L_2^2 + \gamma^2 - L_3^2}{2L_2\sqrt{\varepsilon^2 + \gamma^2}} - \arctan\frac{\gamma}{\varepsilon} \\ \varphi_3 = \arcsin\frac{\varepsilon^2 + L_3^2 + \gamma^2 - L_2^2}{2L_3\sqrt{\varepsilon^2 + \gamma^2}} - \arctan\frac{\gamma}{\varepsilon} \end{cases} \tag{7}$$

where the ε and γ are obtained through Equation (8):

$$\begin{cases} \varepsilon = L_1 \sin\varphi_1 \\ \gamma = L_1 \cos\varphi_1 + L_4 \end{cases} \tag{8}$$

The angular velocities of the AB and BC rods (ω_2 and ω_3) are obtained through Equation (9):

$$\begin{cases} \omega_2 = \frac{L_1L_3\sin\varphi_1\cos\varphi_3 - L_1L_3\cos\varphi_1\sin\varphi_3}{L_2L_3\sin\varphi_2\cos\varphi_3 - L_2L_3\sin\varphi_3\cos\varphi_2}\omega_1 \\ \omega_3 = \frac{L_1L_2\sin\varphi_1\cos\varphi_2 - L_1L_2\cos\varphi_1\sin\varphi_2}{L_2L_3\sin\varphi_3\cos\varphi_2 - L_2L_3\sin\varphi_2\cos\varphi_3}\omega_1 \end{cases} \quad (9)$$

Thus, from the above analysis, we can see the acceleration of point B is related to the crank radius L_1, driving link length L_2, driven rocker 1 length L_3, fixed link length L_4, crank rotational speed ω_1 and the angle of the crank with axis φ_1. That is, the acceleration of the vibrating screen depends on the rod lengths of the vibrating mechanism and the crank rotational speed and position. This provides an important theoretical basis for studying the relationship between the motion law of the vibrating mechanism and time t.

3.2. Acceleration Analysis of Chuanxiong-Soil Residue on Vibrating Screen

The analysis diagram of Chuanxiong-soil residues on a vibrating screen is shown in Figure 3. In this study, the Chuanxiong tuber and soil mixture on the vibrating screen is abbreviated as Chuanxiong-soil residue, and the mass of it is m. In Figure 3a,b, a sloping line refers to the vibrating screen surface, which has an oblique angle α with a horizontal surface; the screen surface coordinate system is established with the residue centroid as the coordinate origin. The x'-axis is along the screen face and upward. The y'-axis is perpendicular to the screen face and upward. The inertial forces of the Chuanxiong-soil residue along the x'-axis direction are $F_{Ix}{}'$ and $F_{Iy}{}'$, respectively. The direction of the inertia force is the same as the acceleration direction of the Chuanxiong-soil residue (opposite to the acceleration direction of the screen surface). When the inertial force is positive, its direction is the positive direction of the x'-axis, and the Chuanxiong-soil residue tends to slide backward (screen tail direction) along the screen surface, which is defined as positive sliding. When the inertia force is negative, its direction is the negative direction of the x'-axis, and the Chuanxiong-soil residue tends to slide advance (screen head direction) along the screen surface, which is defined as negative sliding. When studying the motion features of the Chuanxiong-soil residue relative to the vibrating screen surface, the inertia is considered together with other forces, such as the gravity mg, supporting force F_N, and the friction force F_f. The Chuanxiong-soil residue tends to reach static equilibrium under these forces and the inertia when sliding on the screen surface. Meanwhile, the vibrating mechanism must drive the Chuanxiong-soil residue to slide on the screen. The possible states of the Chuanxiong-soil residue sliding on the screen surface are the positive sliding and the negative sliding, as shown in Figure 3a,b. It is necessary to use dynamics and statics analysis to explore the acceleration of Chuanxiong-soil residues on a vibrating screen.

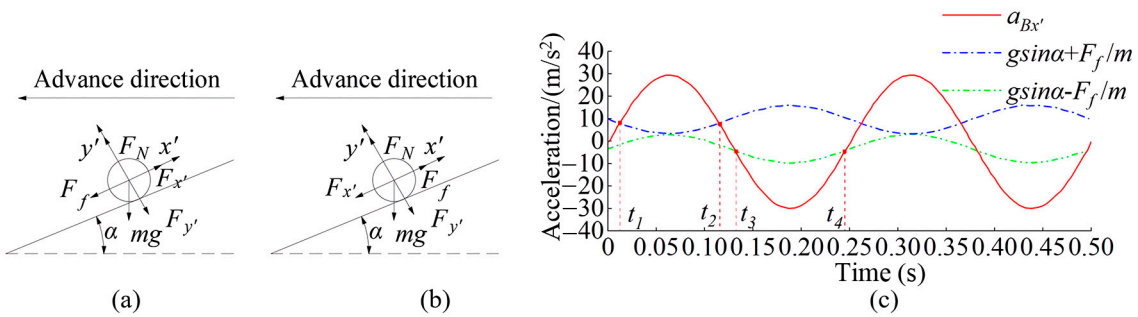

Figure 3. Analysis diagram of Chuanxiong-soil residues on vibrating screen: (**a**) Force analysis of Chuanxiong-soil positive sliding; (**b**) Force analysis of Chuanxiong-soil residue negative sliding; (**c**) The acceleration of the Chuanxiong-soil residue relative to the x'-axis direction of the vibrating screen.

The acceleration of point B in x'-axis and y'-axis directions in the screen surface coordinate system ($a_{Bx'}$ and $a_{By'}$) can be obtained through Equation (10).

$$\begin{cases} a_{Bx'} = -a_{Bx}\cos\alpha - a_{By}\sin\alpha \\ a_{By'} = a_{Bx}\sin\alpha - a_{By}\cos\alpha \end{cases} \tag{10}$$

Substituting the a_{Bx} and a_{By} in Equation (4) into Equation (10), Equation (11) can be obtained as:

$$\begin{cases} a_{Bx'} = (\omega_1^2 L_1\cos\varphi_1 + L_2 a_2\sin\varphi_2 + L_2\omega_2^2\cos\varphi_2)\cos\alpha \\ -(-\omega_1^2 L_1\sin\varphi_1 + L_2 a_2\cos\varphi_2 - L_2\omega_2^2\sin\varphi_2)\sin\alpha \\ a_{By'} = (-\omega_1^2 L_1\cos\varphi_1 + L_2 a_2\sin\varphi_2 + L_2\omega_2^2\cos\varphi_2)\sin\alpha \\ -(-\omega_1^2 L_1\sin\varphi_1 + L_2 a_2\cos\varphi_2 - L_2\omega_2^2\sin\varphi_2)\cos\alpha \end{cases} \tag{11}$$

As shown in Figure 3a, assuming the Chuanxiong-soil residue is in static equilibrium status on the screen in a non-inertial system, it should meet Equation (12):

$$\begin{cases} F_{Ix'} = -ma_{Bx'} = mg\sin\alpha \pm F_f \\ F_N = mg\cos\alpha + F_{y'} = mg\cos\alpha - ma_{By'} \\ F_f = \mu F_N \end{cases} \tag{12}$$

In Equation (12), the sliding friction coefficient of the Chuanxiong-soil residue with steel is $\mu = 0.6$ [25,26]. If $F_{Ix}' = mg\sin\alpha + F_f$, the friction force on the Chuanxiong-soil residue is opposite to the direction of the x'-axis, and the sliding direction of the Chuanxiong-soil residue relative to the vibrating screen is the x'-axis positive direction (Figure 2a). If $F_{Ix}' = mg\sin\alpha - F_f$, the friction force on the screen is the same as the x'-axis direction, and the sliding direction of the Chuanxiong-soil residue relative to the vibrating screen is the x'-axis negative direction (Figure 3b). We can obtain the curve of acceleration $a_{Bx'}$ by substituting the parameters in Table 1 into Equation (4). Similarly, we can obtain the curves of $g\sin\alpha + F_f/m$ and $g\sin\alpha - F_f/m$ by substituting the parameters of the vibrating mechanism into Equations (11) and (12), as shown in Figure 3c.

In Figure 3c, the red solid line represents the curve of $a_{Bx'}$, the blue dotted and dashed line represents the curve of $g\sin\alpha + F_f/m$, and the green dotted and dashed line represents the curve of $g\sin\alpha - F_f/m$. It can be seen that the motion state of the Chuanxiong-soil residue changes with time, which means the position of the crank OA. The acceleration of Chuanxiong-soil residues during positive sliding is always larger than that of the negative sliding in magnitude. The interval of time t_1 to time t_2 represents the positive sliding of the Chuanxiong-soil residue, and the interval of time t_3 to time t_4 represents the negative sliding of the Chuanxiong-soil residue. At the beginning moment of time t_1, the Chuanxiong-soil residue meets $a_{Bx'} = g\sin\alpha + F_f/m$ and starts to experience positive movements until time t_2. The Chuanxiong-soil residue meets $a_{Bx'} = g\sin\alpha - F_f/m$ at time t_3, which is at the beginning of negative direction moments, and the Chuanxiong-soil residue will experience negative movements until time t_4.

3.3. Sliding Speed Analysis of the Chuanxiong-Soil Residue Relative to the Vibrating Screen Surface

To avoid congesting when conveying the Chuanxiong-soil residue, the motion of the Chuanxiong-soil residue on the screen surface along the x'-axis direction needs to be continuous. Thus, the speed of the Chuanxiong-soil residue in the x'-axis direction during the conveying process is analyzed in this section. When the Chuanxiong-soil residue starts to slide into the non-inertial system, its dynamics balance meets Equation (13):

$$m(a_{Bx'} + \dot{v}_{x'}) = mg\sin\alpha \pm F_f \tag{13}$$

where $\dot{v}_{x'}$ is the acceleration of the Chuanxiong-soil residue relative to the vibrating screen, m/s^2.

In Equation (13), the '+' operator is used in positive sliding, and the '−' operator is used in negative sliding. According to the simultaneous Equations (12) and (13), Equation (14) is obtained as:

$$\dot{v}_{x'} = g\sin\alpha - a_{Bx'} \pm \mu(g\cos\alpha - a_{By'}) \tag{14}$$

Substituting $a_{Bx'}$ and $a_{By'}$ in Equation (10) into Equation (14) and integrating time t, the positive sliding speed of the Chuanxiong-soil residue relative to the vibrating screen $v_{x'_1}$ is obtained through Equation (15):

$$\begin{aligned} v_{x'_1} &= \int_{t_1}^{t} g\sin\alpha - a_{Bx'} + \mu(g\cos\alpha - a_{By'})\mathrm{d}t \\ &= g(\mu\sin\alpha - \cos\alpha)(t - t_1) - \int_{t_1}^{t}\left[(\omega_1 L_1\cos\varphi_1 - L_2 a_2\sin\varphi_2 - L_2\omega_2^2\cos\varphi_2)\cos\alpha\right. \\ &\quad \left.+(\omega_1^2 L_1\sin\varphi_1 - L_2 a_2 c\cos\varphi_2 + L_2\omega_2^2\sin\varphi_2)\cos\alpha\right]\mathrm{d}t \end{aligned} \tag{15}$$

Supposing the actual negative sliding starting time is at time $t_{3'}$, the negative sliding speed of the Chuanxiong-soil residue $v_{x'_2}$ can be obtained through Equation (16):

$$\begin{aligned} v_{x'_2} &= \int_{t'_3}^{t} g\sin\alpha - a_{Bx'} - \mu(g\cos\alpha - a_{By'})dt \\ &= -g(\mu\sin\alpha + \cos\alpha)(t - t'_3) - \int_{t'_3}^{t}\left[(\omega_1 L_1\cos\varphi_1 - L_2 a_2\sin\varphi_2 - L_2\omega_2^2\cos\varphi_2)\cos\alpha\right. \\ &\quad \left.+(\omega_1^2 L_1\sin\varphi_1 - L_2 a_2 c\cos\varphi_2 + L_2\omega_2^2\sin\varphi_2)\cos\alpha\right]dt \end{aligned} \tag{16}$$

By substituting the parameters of the vibrating mechanism into Equations (15) and (16) and utilizing MatlabR2020b software, the curve of the positive and negative sliding speed $v_{x'}$ of the Chuanxiong-soil residue relative to the vibrating screen in x'-axis direction can be obtained as shown in Figure 4. It can be seen from Figures 3c and 4 that when the Chuanxiong-soil residue is at point H (t_1 = 0.011 s), the speed and acceleration of the Chuanxiong-soil residue and the vibrating screen are equal, and the Chuanxiong-soil residue meets $F_{Ix'} = mg\sin\alpha + F$. The Chuanxiong-soil residue and the vibrating screen are in a critical state between relative static and relative sliding. After point H, since $F_{Ix'} > mg\sin\alpha + F_f$, the Chuanxiong-soil residue starts to slide positively and accelerate, as shown in point H to point M section. The Chuanxiong-soil residue meets $F_{Ix'} = mg\sin\alpha + F_f$ again at point M (t_2 = 0.115 s). At this moment, the $v_{x'} > 0$ and the Chuanxiong-soil residue reached the maximum positive sliding speed. Since the Chuanxiong-soil residue meets $F_{Ix'} < mg\sin\alpha + F_f$ after point M, the Chuanxiong-soil residue starts to decelerate and slide positively relative to the vibrating screen, as shown in point M to point J section. At point J ($t_{3'}$ = 0.209 s), the instantaneous speed of the Chuanxiong-soil residue and the vibrating screen is equal. The Chuanxiong-soil residue and the vibrating screen are in a critical state between relative static and relative sliding. After point J, since $F_{Ix'} > mg\sin\alpha - F_f$, the Chuanxiong-soil residue accelerates and slides negatively relative to the vibrating screen, as shown in point J to point K section. At point K (t_4 = 0.234 s), since $F_{Ix'} = mg\sin\alpha - F_f$ and $v_{x'} < 0$, the Chuanxiong-soil residue is at its maximum negative sliding speed. After point K, since $F_{Ix'} < mg\sin\alpha - F_f$, the Chuanxiong-soil residue starts to decelerate and slide negatively, as shown in point K to point Q section. When the Chuanxiong-soil residue meets $F_{Ix'} = mg\sin\alpha - F_f$ instantaneously at point Q ($t_{1'}$ =0.264 s), the Chuanxiong-soil residue and the vibrating screen are in the critical state between relative static and relative sliding again, and a cycle of sliding is completed. The area enveloped by the curve *HMJ* and the time axis with a speed of 0 represents the positive sliding distance of the Chuanxiong-soil residue relative to the vibrating screen. The area enveloped by the curve *JKQ* and the time axis with a speed of 0 represents the negative sliding distance of the Chuanxiong-soil residue relative to the vibrating screen. It can be seen that the area enclosed by the curve *HMJ* is larger than the area enclosed by the curve *JKQ*. This indicated that the positive sliding distance of the Chuanxiong-soil residue is greater than the negative sliding distance in a cycle. The motion meets the requirements of positive (backward) conveying of the Chuanxiong-soil residues to avoid congestion on the vibrating screen.

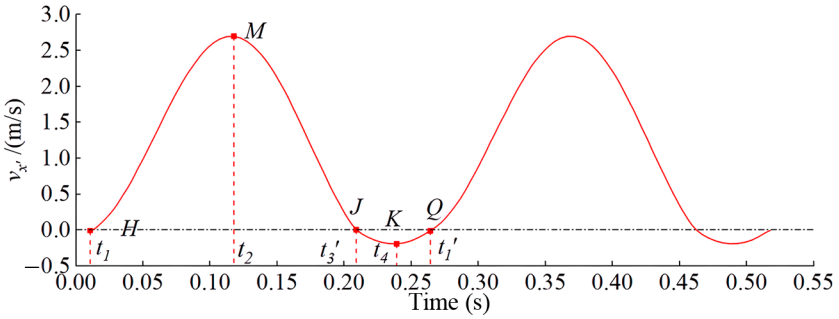

Figure 4. The curve of the positive and negative sliding speed of the Chuanxiong-soil residue relative to the vibrating screen in the x'-axis direction.

3.4. Motion Analysis of the Chuanxiong-Soil Residue Thrown Upwards by the Vibrating Screen

The motion of Chuanxiong-soil residue after being thrown upwards includes the x'-axis direction and y'-axis direction; thus, the velocities of the Chuanxiong-soil residue after being thrown upwards and falling back to collide with the vibrating screen were studied in this section. According to static equilibrium Equation (12), it can be obtained that the critical condition for the Chuanxiong-soil residue to be thrown and leave the vibrating screen is $F_N = 0$ (i.e., the positive pressure of the Chuanxiong-soil residue to the vibrating screen is 0). Equation (17) can be obtained as:

$$a_{By'} = -g\cos\alpha \tag{17}$$

Substituting the $a_{By'}$ in Equation (11) to Equation (17), Equation (18) can be obtained as:

$$(-\omega_1^2 L_1\cos\varphi_1 + L_2 a_2\sin\varphi_2 + L_2\omega_2^2\cos\varphi_2)\sin\alpha - (-\omega_1^2 L_1\sin\varphi_1 + L_2 a_2\cos\varphi_2 - L_2\omega_2^2\sin\varphi_2)\cos\alpha + g\cos\alpha = 0 \tag{18}$$

Substituting Equations (5)–(9) into Equation (18), we can see the Chuanxiong-soil residue leaves the vibrating screen at time t_0 (=0.04 s). For the Chuanxiong-soil residue, it can be seen from Figure 4 that the time of being thrown upwards is greater than the time of starting positive movements, namely t_0 (=0.04 s) > t_1 (=0.011 s), the Chuanxiong-soil residue will move positively relative to the vibrating screen before it leaves the screen at time t_0.

Through the throw analysis of the Chuanxiong-soil residue, when the vibrating screen throws Chuanxiong-soil residue into the air along the x'-axis positive direction, Equation (19) can be obtained as:

$$\begin{cases} m(a_{Bx'} + a'_{x'}) = -mg\sin\alpha \\ m(a_{By'} + a'_{y'}) = -mg\cos\alpha \end{cases} \tag{19}$$

where $a'_{x'}$ and $a'_{y'}$ are the acceleration of Chuanxiong-soil residue in the x'-axis and y'-axis directions relative to the vibrating screen after throwing the Chuanxiong-soil residue by the vibrating screen, m/s^2.

Substituting Equation (11) into Equation (19), after the Chuanxiong-soil residue is thrown upwards, the acceleration of it relative to the vibrating screen in the x'-axis and y'-axis directions (α'x′ and α'y′) can be obtained through Equation (20):

$$\begin{cases} a'_{x'} = (\omega_1^2 L_1\cos\varphi_1 + L_2 a_2\sin\varphi_2 + L_2\omega_2^2\cos\varphi_2)\cos\alpha \\ -(-\omega_1^2 L_1\sin\varphi_1 + L_2 a_2\cos\varphi_2 - L_2\omega_2^2\sin\varphi_2)\sin\alpha - g\sin\alpha \\ a'_{y'} = (-\omega_1^2 L_1\cos\varphi_1 + L_2 a_2\sin\varphi_2 + L_2\omega_2^2\cos\varphi_2)\sin\alpha \\ -(-\omega_1^2 L_1\sin\varphi_1 + L_2 a_2\cos\varphi_2 - L_2\omega_2^2\sin\varphi_2)\cos\alpha - g\cos\alpha \end{cases} \tag{20}$$

After the Chuanxiong-soil residue is thrown upwards, by integrating Equation (20) with time t, the velocity of the Chuanxiong-soil residue relative to the x'-axis and y'-axis directions of the vibrating screen ($v'_{x'}$ and $v'_{y'}$) is obtained through Equation (21):

$$\begin{cases} v'_{x'} = v'_0 - \int_{t_0}^{t} \left[\begin{array}{l} (\omega_1^2 L_1 \cos\varphi_1 + L_2 a_2 \sin\varphi_2 + L_2\omega_2^2 \cos\varphi_2)\cos\alpha \\ +(-\omega_1^2 L_1 \sin\varphi_1 + L_2 a_2 \cos\varphi_2 - L_2\omega_2^2 \sin\varphi_2)\sin\alpha + g\sin\alpha \end{array} \right] \mathrm{d}t \\ v'_{y'} = v'_{0\mathrm{y}} - \int_{t_0}^{t} \left[\begin{array}{l} (-\omega_1^2 L_1 \cos\varphi_1 + L_2 a_2 \sin\varphi_2 + L_2\omega_2^2 \cos\varphi_2)\sin\alpha \\ +(-\omega_1^2 L_1 \sin\varphi_1 + L_2 a_2 \cos\varphi_2 - L_2\omega_2^2 \sin\varphi_2)\cos\alpha + g\cos\alpha \end{array} \right] \mathrm{d}t \end{cases} \quad (21)$$

where v'_0 is the speed of Chuanxiong-soil residue in the x'-axis direction relative to the vibrating screen after being thrown upwards, m/s; v'_{0y} is the speed of Chuanxiong-soil residue in the y'-axis direction relative to vibrating screen after being thrown upwards, m/s.

At the beginning of throwing the Chuanxiong-soil residue upwards, the value of v'_{0y} is 0 m/s. Since t_0 is in the positive sliding range at the time of throwing the Chuanxiong-soil residue upwards, the positive sliding velocity equation of the Chuanxiong-soil residue relative to the vibrating screen is met. Substituting t_0 to Equation (15), we can obtain that v'_0 = 0.693 m/s. By integrating $v'_{y'}$ in Equation (21) with time t, the displacement of the Chuanxiong-soil residue relative to the y'-axis direction of the vibrating screen can be obtained as:

$$S'_{y'} = -\int\int_{t_0}^{t} \left[\begin{array}{l} (-\omega_1^2 L_1 \cos\varphi_1 + L_2 a_2 \sin\varphi_2 + L_2\omega_2^2 \cos\varphi_2)\sin\alpha \\ +(-\omega_1^2 L_1 \sin\varphi_1 + L_2 a_2 \cos\varphi_2 - L_2\omega_2^2 \sin\varphi_2)\cos\alpha + g\cos\alpha \end{array} \right] \mathrm{d}t\mathrm{d}t \quad (22)$$

From Equation (22), we can see the Chuanxiong-soil residue is back to the vibrating screen when its relative displacement to the vibrating screen $S'_{y'}$ is 0. Then, we can obtain time t' (=0.18 s) when Chuanxiong-soil residue falls back to hit the vibrating screen through Equation (22). The motion curve of the Chuanxiong-soil residue, from being thrown upwards to falling on the vibrating screen, is plotted by Matlab2020b, as shown in Figure 5a. When the Chuanxiong-soil residue is being thrown upwards from the vibrating screen, it firstly accelerates in the positive direction of the y'-axis and reaches the maximum speed v_{2y} (about 0.975 m/s) in the y'-axis direction at time t_5. After time t_5, the speed of Chuanxiong-soil residue decelerates until it falls back on the vibrating screen at time t' with the speed of $v'_{y'}$ (about −2.135 m/s). The velocity ($v'_{x'}$) of the Chuanxiong-soil residue along the x'-axis direction at time t' is obtained as 1.784 m/s by substituting the value of t' to the Equation (21).

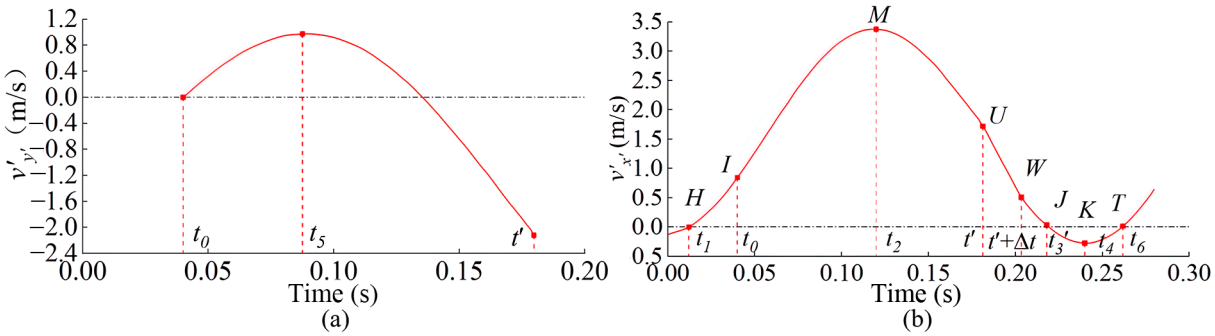

Figure 5. Velocities of the Chuanxiong-soil residue after being thrown upwards and falling back to collide with the vibrating screen: (**a**) Velocity in the y'-axis direction; (**b**) Velocity in the x'-axis direction.

When the Chuanxiong-soil residue falls back onto the vibrating screen, the Chuanxiong-soil residue will collide with the vibrating screen. Assuming the collision time is Δt, and the velocity restitution coefficient factor after the collision is 0, the relative speed of

the Chuanxiong-soil residue in the y'-axis direction after the collision is $v'_{y'}(t' + \Delta t) = 0$. Equation (23) can be obtained according to the momentum theorem [27].

$$v'_{x'}(t' + \Delta t) = \begin{cases} 0 & \left|v'_{x'}(t')\right| \le -\mu v'_{y'}(t') \\ v'_{x'}(t') + \frac{v'_{x'}(t')}{\left|v'_{x'}(t')\right|}\mu v'_{y'}(t') & \left|v'_{x'}(t')\right| > -\mu v'_{y'}(t') \end{cases} \quad (23)$$

where $v'_{x'}(t')$ and $v'_{y'}(t')$ are the velocities in x'-axis and y'-axis directions relative to the vibrating screen before collision, m/s; $v'_{x'}(t' + \Delta t)$ is the speed relative to the x'-axis direction of the vibrating screen after collision, m/s.

For the value of μ is 0.6, the $\left|v'_{x'}(t')\right|$ is greater than $-\mu v'_{y'}(t')$, that is 1.784 > 1.281. Previous studies [28,29] showed that since the collision process between the soil and the steel bar on the vibrating screen is viscoelastic deformation, the instantaneous impact of the Chuanxiong-soil residue falling on the steel bar is simplified as a shear force. The Chuanxiong-soil residue volumetric weight is 1.2 g/cm^3. The Chuanxiong-soil residue is regarded as a sphere with a diameter of 50 mm, and the volume weight of Chuanxiong-soil residue M is 628 g. Combined with the actual situation of the Chuanxiong-soil residue, the collision area is about 150 mm^2, and the collision time Δt (The main topic in this study is the convey motion of Chuanxiong-soil residue on the screen. Although the collision period exists in the entire cycle, the calculation method was not discussed in this study and will be specially discussed in our next study). We can obtain the speed of the Chuanxiong-soil residue relative to the x-axis direction of the vibrating screen after the collision through Equation (23) as $v'_{x'}(t' + \Delta t) = 0.503$ m/s. Substituting the parameters of the vibrating mechanism into Equations (21) and (23), the velocity curve $v'_{x'}$ of the Chuanxiong-soil residue relative to the x'-axis direction of the vibrating screen is obtained as shown in Figure 5b.

According to Figures 4 and 5, it can be seen that the acceleration of the Chuanxiong-soil residue at point H ($t_1 = 0.011$ s) is identical to that of the vibrating screen, and the Chuanxiong-soil residue starts to accelerate and slide positively. During this process, the speed and displacement of the Chuanxiong-soil residue relative to the vibrating screen are greater than 0. When the Chuanxiong-soil residue moves to point I ($t_0 = 0.04$ s) in Figure 5a, it is thrown upwards from the screen surface with the speed of v_0 (about 0.693 m/s) in Figure 5b. During the process of being thrown upwards, because the acceleration of the Chuanxiong-soil residue is greater than 0, the Chuanxiong-soil residue continues to make a positive acceleration movement relative to the vibrating screen. Until point M ($t_2 = 0.120$ s) in Figure 5b, the Chuanxiong-soil residue reaches the maximum speed (about 3.350 m/s). After point M, the Chuanxiong-soil residue experiences a deceleration movement until it falls back to hit the vibrating screen (at point U in Figure 5b). The time when the Chuanxiong-soil residue falls on screen is $t' = 0.18$ (Figure 5a), and the collision end time is $t' + \Delta t = 0.204$ s at point W, as shown in Figure 5b. After the collision, since $F_{x'} < mg\sin\alpha + F_f$ and $v'_{x'}(t' + \Delta t) > 0$, the Chuanxiong-soil residue continues to slow down and slide along the positive direction of x'-axis until point J ($t_{3'} = 0.209$ s) in Figure 5b. The speed of Chuanxiong-soil residue is 0 at point J. At this moment, since $F_{x'} > mg\sin\alpha - F_f$, the Chuanxiong-soil residue will slide and accelerate along the negative direction until it reaches a maximum negative speed at point K ($t_4 = 0.234$ s), where $F_{x'} = mg\sin\alpha - F_f$. After point K, because $F_{x'} < mg\sin\alpha - F_f$, the Chuanxiong-soil residue will start to decelerate until point T ($t_6 = 0.261$ s). Finally, the Chuanxiong-soil residue completes a cycle movement. It can be seen that, within a cycle, the motion process of the Chuanxiong-soil residue is divided into six steps such as positive acceleration sliding (HJ), throwing upwards (IMU), collision (UW), positive deceleration sliding (WJ), negative acceleration sliding (JK) and negative deceleration sliding (KT).

3.5. Conveying Distance Analysis of the Chuanxiong-Soil Residue Relative to the Screen in a Motion Cycle

We can see from Figure 5b that the Chuanxiong-soil residue moves in a positive direction relative to the vibrating screen from time t_1 to time t_0 (0.011~0.04 s). The sliding distance of the Chuanxiong-soil residue along the x'-axis positive direction of the vibrating screen during this period S_1 is obtained through Equation (24):

$$S_1 = \int_{t_1}^{t_0} v_{x'_1} \mathrm{d}t = \int \int_{t_1}^{t_0} g \sin\alpha - a_x + \mu(g\cos\alpha - a_y)\mathrm{d}t^2 \tag{24}$$

When the Chuanxiong-soil residue is thrown upwards by the vibrating screen from time t_0 to time t' (0.04~0.18 s), the moving distance S_2 of the Chuanxiong-soil residue along the x'-axis positive direction of the vibrating screen is obtained through Equation (25):

$$\begin{array}{l} S_2 = \int_{t_0}^{t'} v'_{x'} \mathrm{d}t \\ = \int_{t_0}^{t'} \left\{ v'_0 - \int_{t_0}^{t'} \left[\begin{array}{l} (\omega_1^2 L_1 \cos\varphi_1 - L_2 a_2 \sin\varphi_2 - L_2\omega_2^2 \cos\varphi_2)\cos\alpha \\ +g\sin\alpha \end{array} \right] \mathrm{d}t \right\} \mathrm{d}t \end{array} \tag{25}$$

The Chuanxiong-soil residue collides with the vibrating screen in the time interval of t'~$t' + \Delta t$ (about 0.18~0.204 s). The conveying distance of the Chuanxiong-soil residue during this period is very small and ignored in this study. The Chuanxiong-soil residue moves positively on the vibrating screen in the time interval of $t' + \Delta t$~t'_3 (0.204~0.209 s), and the moving distance S_3 of the Chuanxiong-soil residue along the x'-axis positive direction of the vibrating screen during this period is obtained through Equation (26):

$$\begin{array}{l} S_3 = \int_{t'+\Delta t}^{t'_3} v_{x'_1} \mathrm{d}t = \int_{t'+\Delta t}^{t'_3} \{ g(\mu\sin\alpha - \cos\alpha)(t - t_1) - \\ \int_{t_1}^{t'_3} \left[(\omega_1 L_1 \cos\varphi_1 - L_2 a_2 \sin\varphi_2 - L_2\omega_2^2 \cos\varphi_2)\cos\alpha \right. \\ \left. +(\omega_1^2 L_1 \sin\varphi_1 - L_2 a_2 c \cos\varphi_2 + L_2\omega_2^2 \sin\varphi_2)\cos\alpha \, \mathrm{d}t \right] \} \mathrm{d}t \end{array} \tag{26}$$

The Chuanxiong-soil residue moves in a negative direction in the time interval of t'_3~t_6 (0.209~0.261 s), and the sliding distance S_4 of the Chuanxiong-soil residue along the x'-axis negative direction of the vibrating screen is obtained through Equation (27):

$$\begin{array}{l} S_4 = \int_{t'_3}^{t_6} v_{x'_2} \mathrm{d}t = \int_{t'_3}^{t_6} \{ -g(\mu\sin\alpha + \cos\alpha)(t - t_1) \\ - \int_{t'_3}^{t_6} \left[(\omega_1 L_1 \cos\varphi_1 - L_2 a_2 \sin\varphi_2 - L_2\omega_2^2 \cos\varphi_2)\cos\alpha \right. \\ \left. +(\omega_1^2 L_1 \sin\varphi_1 - L_2 a_2 c \cos\varphi_2 + L_2\omega_2^2 \sin\varphi_2)\cos\alpha \right] \mathrm{d}t \} \mathrm{d}t \end{array} \tag{27}$$

According to the motion process of the Chuanxiong-soil residue in a cycle, the motion distance of the Chuanxiong-soil residue along the x'-axis direction of the vibrating screen in a rotation cycle is obtained through Equation (28):

$$S_\xi = S_1 + S_2 + S_3 - S_4 \tag{28}$$

Substituting the parameters of the vibrating mechanism and t_1, t_0, t', t'_3, t_6 (0.011 s, 0.04 s, 0.18 s, 0.209 s, 0.261 s) into Equation (28), we can see the motion displacement of the Chuanxiong-soil residue along the x'-axis positive direction of the vibrating screen in a cycle is obtained through Equation (29):

$$S_\xi = 0.01246 + 0.36459 + 0.00381 - 0.00561 \approx 0.410 \text{ m} \tag{29}$$

It can be seen from Figure 3a,b that the advancement direction of the Chuanxiong harvester is opposite to the positive sliding direction of the Chuanxiong-soil residue. The included angle between the positive sliding direction of the Chuanxiong-soil residue and the horizontal direction is α (20°). The advancement speed of the Chuanxiong harvester is 0.5 m/s. Since the n is 240 r/min (4 r/s or 0.25 s per round), the advancement distance

of the Chuanxiong harvester in the horizontal direction is S_R = 0.125 m in a rotation cycle. Thus, the advancement distance of the Chuanxiong harvester in the x'-axis direction S'_R in a cycle can be obtained through Equation (30)

$$S'_R = \frac{S_R}{\cos\alpha} = 0.133 \tag{30}$$

When considering the advancement speed of the Chuanxiong harvester, the absolute movement distance of the Chuanxiong-soil residue on the screen along the x'-axis positive direction in a cycle ΔS is obtained through Equation (31):

$$\Delta S = S_{\xi} - S'_R = 0.277 \tag{31}$$

Since $\Delta S > 0$, there will be nearly no soil blocking during the harvesting process. However, because the advancement speed of the harvester is different, the faster the speed may lead to soil blocking. According to Equation (31), the suitable working speed of the Chuanxiong harvester v_R should meet $S_{\xi} - 0.25v_R/\cos\alpha = 0$. Thus, $v_R < 1.541$ m/s.

4. Simulation and Results Analysis

The DEM analysis method has been widely used to study the movement of particles on vibrating screens [30,31]. The coupling simulation method of EDEM and RecurDyn was commonly used in solving complex motion-related problems in the agricultural industry [32,33]. The conveying process of the Chuanxiong-soil residue on the vibrating screen was analyzed by using the coupling simulation of EDEM2020 and RecurDynV9R4. The crankshaft rocker vibrating mechanism model was constructed by SolidWorks2016 and imported into the RecurdynV9R4 software by x_t file, as shown in Figure 6. The rotational assemblies, advancement speed, and rotational speed of the crank rod were defined in the RecurdynV9R4. In the construction of the RecurDyn simulation environment, the advancement velocity of the entire frame of the vibrating screen was set to 1.5 m/s. The crank rotational speed was set to 240 r/min. A step function was used to define the motion.

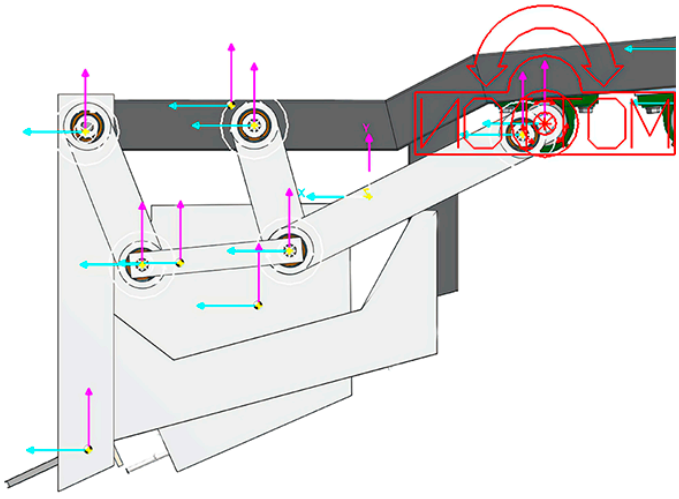

Figure 6. Simulation model in RecurDyn.

Then, the main parts of the vibrating screen were defined as Walls and exported as an 'EDEM.wall' file by the External SPI function. The document was imported into EDEM software, as shown in Figure 7. The geometric dimensions and physical and mechanical properties of chuanxiong tubers were obtained through a series of experiments using the INSTRON5544 universal material testing machine and other equipment. The basic parameters of soil were cited from another study [34]. The parameters of materials used in this study are shown in Table 2. The contacting parameters are shown in Table 3.

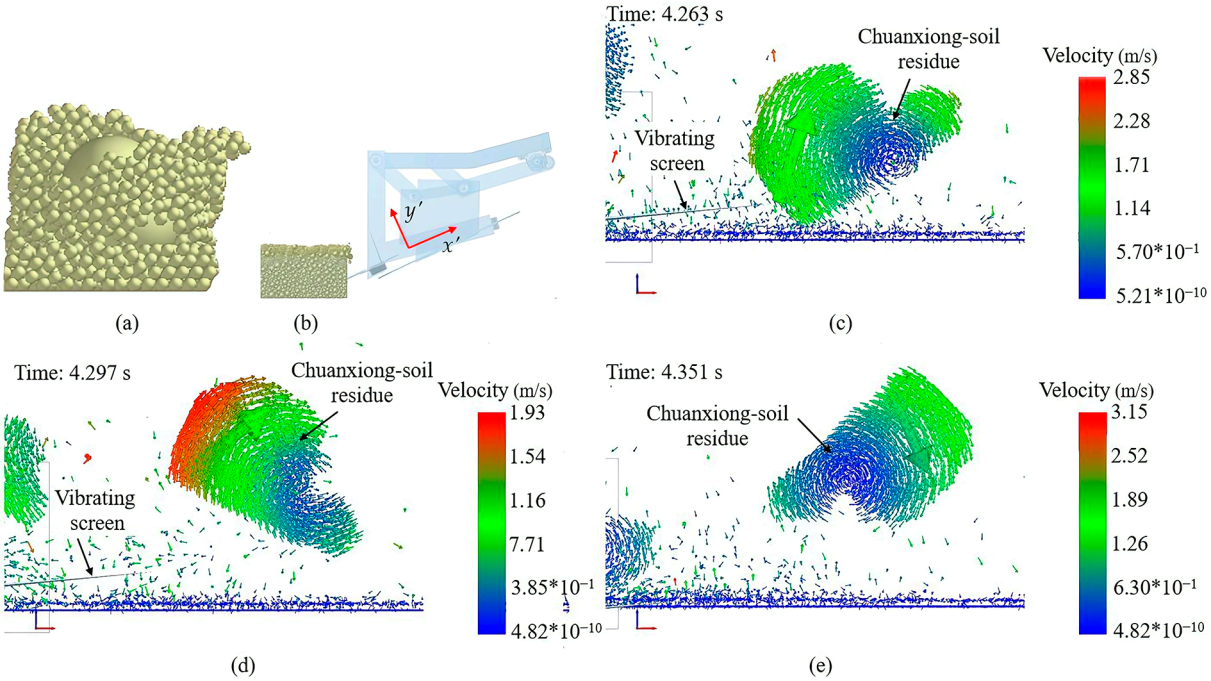

Figure 7. EDEM simulation process: (**a**) Simulation model of Chuanxiong and soil; (**b**) EDEM overall simulation model; (**c**) Motion of the Chuanxiong-soil residue at leaving screen moment; (**d**) Motion of the Chuanxiong-soil residue at throwing moment; (**e**) Motion of the Chuanxiong-soil residue at biggest velocity moment.

Table 2. Material parameters used in the simulation.

Parameter Name	Soil	Chuanxiong-Soil Residue	Vibrating Screen
Poisson's ratio	0.35	0.32	0.31
Shear modulus (Pa)	1×10^6	2×10^{10}	7×10^{10}
Density (kg/m^3)	1722	1230	7800

Table 3. Contacting parameters used in the simulation.

Parameter Name	Soil	Chuanxiong-Soil Residue
Soil—Chuanxiong	Dynamic friction factor	1.06
	Static friction factor	0.34
	Restitution factor	0.136
Soil—45 Steel	Dynamic friction factor	0.04
	Static friction factor	0.5
	Restitution factor	0.28
Soil—Soil	Dynamic friction factor	0.2
	Static friction factor	0.5
	Restitution factor	0.2
Chuanxiong—45 Steel	Dynamic friction factor	1.07
	Static friction factor	0.2
	Restitution coefficient	0.177

The Chuanxiong-soil residue on the screen is solid particle material. The soil in the Chuanxiong planting area is common clay soil, which causes the tubers and soil to stick together and difficulty separate. When it moves on the screen surface, it is composed of a series of discrete independent units of the mixture on the screen. The Chuanxiong-soil residue itself has a certain shape and size, and its motion conforms to Newton's second law, so it is feasible to analyze the motion of the particles on the screen surface using the discrete element method. The Chuanxiong-soil residue on the screen is solid particle material.

According to our statistics calculation, the diameter of the Chuanxiong-soil residue was about 100 mm on average. The average depth of Chuanxiong tuber centroid under the soil was about 10–50 mm. To simplify the simulation, the Chuanxiong-soil residue was constructed as a sphere with a diameter of 100 mm. The soil particles were constructed as spheres with diameters of 10 mm, 20 mm, and 30 mm, respectively. The Hertz–Mindlin and Standard Rolling Friction models were used to construct the simulation model. The particle plant was set as a cuboid with 3750 mm width, 7200 mm length, and 200 mm height. The particle plant generated a total of 100,000 mixtures at a rate of 5000 per second. The simulation time was taken as 8 s. The centroids of Chuanxiong-tubers were randomly distributed within the soil at depths ranging from 10 mm to 50 mm from the soil surface. The excavating depth of the Chuanxiong harvester was set to 130 mm. The EDEM simulation process is shown in Figure 7.

Figure 7a is the constructed Chuanxiong and soil simulation model. Figure 7b is the constructed EDEM overall simulation model. In Figure 7c, the Chuanxiong-soil residue was just leaving the screen, and the corresponding time was about 4.263 s. In Figure 7d, the Chuanxiong-soil residue was thrown upwards, and the corresponding time was about 4.297 s. In Figure 7e, the Chuanxiong-residue reached a maximum speed, and the corresponding time was about 4.351 s. From Figure 7c–e, we can see the Chuanxiong-soil residue rotated and moved in the direction of the vibration screen.

In Figure 7c, the Chuanxiong-soil residue was sliding to leave the vibrating screen, and the corresponding time was at 4.263 s. In Figure 7d, the Chuanxiong-soil residue was thrown upwards by the vibrating screen, and the corresponding time was about 4.297 s. In Figure 7e, the Chuanxiong-soil residue reached a maximum speed, and the corresponding time was about 4.351 s. From Figure 7c–e, a green solid arrow in the Chuanxiong-soil residue represented the direction of the velocity vector, which indicated that the residue slid and was thrown upwards while rotating clockwise. Compared with Figure 7c, it can be seen that the Chuanxiong-soil residue in Figure 7e was moved further away from the vibrating screen.

The time consumption for the Chuanxiong-soil residue from the time of leaving the screen to reaching the maximum velocity was about 0.075 s (from 4.263 s in Figure 7c to 4.351 s in Figure 7e), which was nearly consistent with the theoretical analysis (t_2–t_0 = 0.075 s). Throughout this process, the overall movement of the Chuanxiong-soil residue towards the conveying direction with regard to the screen showed no congestion phenomenon. The simulation results indicated the theoretical analyses of the Chuanxiong-soil residue motion process were valid.

The speed curves of the Chuanxiong-soil residue and vibrating screen along the x'-axis direction in the simulation are shown in Figure 8. The red solid line represents the velocity of Chuanxiong-soil residue in the x'-axis direction. The blue dashed line represents the velocity of the vibrating screen in the x'-axis direction. We can see that the speed of the Chuanxiong-soil residue changed over time. When the Chuanxiong-soil residue was at point A_1, it was relatively static with the vibrating screen. After that, the moving speed of the Chuanxiong-soil residue gradually increased and was greater than the moving speed of the vibrating screen, and the overall motion of the Chuanxiong-soil residue was in a positive acceleration state. At point A_2, the Chuanxiong-soil residue started to leave the screen. The speed of the Chuanxiong-soil residue in the x'-axis direction increased to about 3.70 m/s at point A_3. Then, it started to decelerate until it fell back to the screen surface, causing a collision in the point A_4 to point A_5 section. After the collision, the Chuanxiong-soil residue continued to decelerate until point A_6. After point A_6, the speed of Chuanxiong-soil residue relative to the vibrating screen was 0 m/s. The moving speed of the vibrating screen was greater than that of the Chuanxiong-soil residue, and the Chuanxiong-soil residue was in a state of negative acceleration sliding. The negative sliding speed of the Chuanxiong-soil residue reached a maximum at point A_7. After point A_7, the negative sliding speed of the Chuanxiong-soil residue decelerated until point A_8. Throughout this process, the area enclosed by the velocity curve of the Chuanxiong-soil residue and the time axis with the

velocity of 0 was larger than the area enclosed by the velocity curve of the vibrating screen and the time axis with the velocity of 0, indicating that the overall positive sliding distance of the Chuanxiong-soil residue was larger than the advancement moving distance of the vibrating screen. Therefore, the Chuanxiong-soil residue can be effectively conveyed on the screen in the x'-axis positive direction.

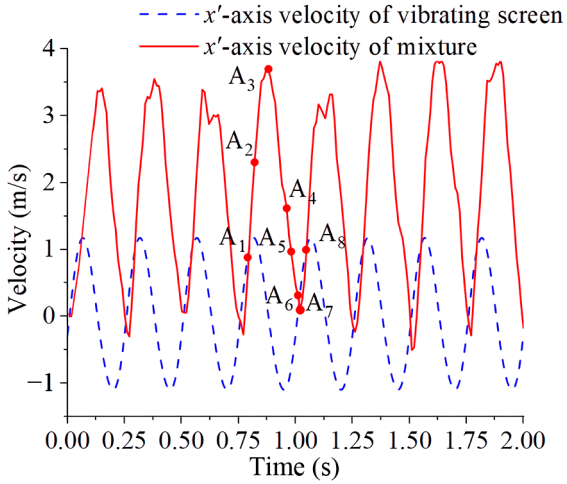

Figure 8. Velocities of the Chuanxiong-soil residue and vibrating screen in the x′-axis direction.

In Figure 8, we can see the maximum speed of Chuanxiong-soil residue along the x'-axis direction was about 3.5 m/s on average, which is close to the theoretical analysis of v_2 = 3.35 m/s in Figure 5b, and the error was insignificant. The error was mainly caused by the unstable velocity after the collision. These analyses of the simulation results indicated that the theoretical motion process analysis of the Chuanxiong-soil residue on the screen was valid.

5. Field Tests

5.1. Test of Chuanxiong-Soil Residue Motion Data

During the experiment, a 3D accelerometer was fixed on the fixed link center of the vibrating sieve by using a sensor adhesive wax and connected to the computer via a data cable, as shown in Figure 9a. In the axis setting process, the positive direction of the x_f-axis was horizontal to the left of the vibrating screen. The positive direction of y_f-axes was vertically upward. The z_f-axis was perpendicular to the x-axis and y-axis and pointed towards the left side of the harvester. During the test, the entire harvester was hanged on a CL904 tractor. The testing process is as follows: First, the sensors were installed on the vibrating screen, and the tractor lifted the Chuanxiong harvester. Then, the output shaft of the tractor was started, and the crank rotational speed of the harvester was adjusted to about 240 r/min by adjusting the hand throttle. A tachometer was used to measure the crank rotational speed. Once the rotational speed of the crank reached 240 r/min and stabilized, the computer began to record acceleration data of the vibrating screen for about 10 s. These recorded video data were imported into the TEMA2019 software for data processing. The motion law test results are shown in Figure 9b,c.

According to the experimental video analysis, we found no congestion of Chuanxiong-soil residues on the vibration screen. There was no doubt that the positive moving distance of the Chuanxiong-soil residue was always greater than the negative moving distance of the Chuanxiong-soil residue under the action of the vibrating screen. In Figure 9b,c, the velocity along the x'-axis direction was greater than the velocity along the y'-axis direction, and the velocity curves were similar to the theoretical analysis.

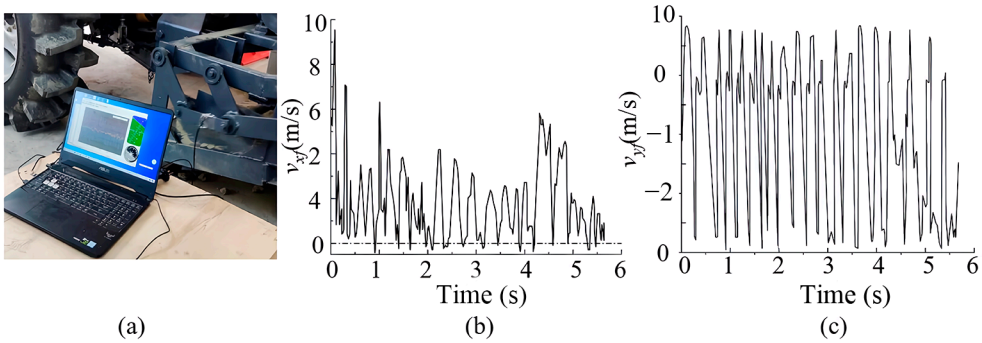

Figure 9. Motion law test: (**a**) Motion data test; (**b**) The velocity of the Chuanxiong-soil residue along the x'-axis direction of the vibrating screen; (**c**) The velocity of the Chuanxiong-soil residue along the y'-axis direction of the vibrating screen.

5.2. Field Test of Chuanxiong-Soil Conveying Ability

The test was conducted in Pengzhou Sichuan, China, a typical Chuanxiong planting region, as shown in Figure 10. Since the designed working speed of the harvester is faster than 0.5 m/s, to verify the actual working performance of the vibrating screen, four harvester advancement speeds (0.5 m/s, 1 m/s, 1.5 m/s, and 2 m/s) and two crank rotational speeds (0 r/min, 120 r/min, and 240 r/min) were tested in the field. When the crank rotational speed was 0 r/min, the vibrating screen did not work. The advancement distance of Chuanxiong harvester in every testing group was 10 m. If the harvester could not maintain a good working efficiency, the test was ended. Before starting the field tests, the Chuanxiong and soil mixture were removed. After the test, the Chuanxiong and soil remaining on the vibrating screen were weighed and recorded. The testing results are shown in Table 4. The weight of the Chuanxiong and soil on the screen after the working process served as the criterion for evaluating the conveyance performance of the vibrating screen.

Figure 10. Harvesting test: (**a**) Without congestion; (**b**) With congestion.

From Table 4, we can see there was a significant difference in the mass of the Chuanxiong-soil residue when the crank of the vibrating screen was working compared with when it was not. The field tests showed that the vibrating screen obviously reduced the soil congestion on the screen. The harvesting depth, harvesting width, and vibrating screen length of the Chuanxiong harvester are about 130 mm, 1600 mm, and 300 mm, respectively. Theoretically, ignoring the loss of soil, the vibrating screen can contain about 107.5 kg of soil if no congestion occurs. The Chuanxiong harvester smoothly finished the harvesting work without any congestion in testing groups 1, 4, and 7 (as shown in Figure 10a). However, in testing groups 2, 3, 5, 6, 8, 9, 10, 11, and 12, the vibrating screen became congested with excess soil and Chuanxiong tuber mixture, and the Chuanxiong harvester faced difficulty functioning or even failed to function (as shown in Figure 10b). From Table 4, we can see that when the crank rotated at a speed of 240 r/min, and the advancement speed did not exceed 1.5 m/s, the weights of Chuanxiong and the soil on the screen after the test were below 107.5 kg. However, the weights were greater than 107.5 kg when the rotational speed

of the crank was slower than 240 r/min. This verified the conveyance performance of the vibrating screen. The field tests verified the theoretical analysis, and the appropriate advancement speed was varied from 0.5 m/s to 1.5 m/s.

Table 4. Field testing results.

Testing Group	Advancement Speed (m/s)	Crank Rotational Speed (r/min)	Chuanxiong and Soil Weight (kg)
1	0.5	240	71.5
2	0.5	120	140.195
3	0.5	0	183.4
4	1	240	84.7
5	1	120	163.405
6	1	0	212.4
7	1.5	240	105.7
8	1.5	120	185.625
9	1.5	0	231.8
10	2	240	185.8
11	2	120	205.92
12	2	0	258.6

6. Conclusions

In this study, a more comprehensive study was conducted on the motion of the Chuanxiong-soil residue and a crankshaft rocker vibrating mechanism. The models for studying the movement process of Chuanxiong-soil residue and vibration screen were established, considering both speed and acceleration. The theoretical analysis results showed that the motion process of the Chuanxiong-soil residue on the vibrating screen in one rotation cycle was divided into six steps such as positive acceleration sliding, throwing upwards, collision, positive deceleration sliding, negative acceleration sliding, and negative deceleration sliding. From the theoretical analysis, we can see the positive moving distance of the Chuanxiong-soil residue was greater than the negative distance. Theoretically, to prevent soil congestion during the harvesting process, the working speed of the Chuanxiong harvester should be slower than 1.5 m/s. The simulation results proved the theoretical analysis was valid and indicated the conveyance ability of the vibrating screen was good. Through the analysis of the simulation and field test results, it was obvious that the theoretical motion process analysis of Chuanxiong-soil residues on the screen was valid. The Chuanxiong-soil residues were effectively conveyed backward without any congestion when the vibrating screen functioned, and the advancement speed was 1.5 m/s.

Author Contributions: Conceptualization, J.W. and Y.Y.; methodology, J.W.; software, J.W.; validation, M.L., Y.Y. and H.X.; formal analysis, R.C.; investigation, J.W.; resources, M.L.; data curation, Y.Y. and J.L.; writing—original draft preparation, J.W.; writing—review and editing, J.W.; visualization, J.W.; supervision, M.L.; project administration, M.L.; funding acquisition, M.L. All authors have read and agreed to the published version of the manuscript.

Funding: This research was funded by Scientific and technological research of the Sichuan Province Pharmaceutical Administration and Technology Program, grant number (2021MS025), Chengdu Science and Technology Program (2021-YF05-00075-SN), and Agricultural Mechanization Weak Process.

Data Availability Statement: The data that support the findings of this study are available on request from the corresponding author.

Acknowledgments: The authors gratefully acknowledge the editors and anonymous reviewers for their constructive comments on our manuscript.

Conflicts of Interest: The authors declare no conflicts of interest.

References

1. Wang, P.Q.; Hao, D.L.; Xiong, X.J. Anti-hypertension effect of Wuwei Jiangya decoction via ACE2/Ang1-7/MAS signaling pathway in SHR based on network degree-distribution analysis. *Ethnopharmacology* **2024**, *319*, 17. [CrossRef]
2. Chen, Z.J.; Zhang, C.; Gao, F.; Fu, Q.; Fu, C.M.; He, Y.; Zhang, J.M. A systematic review on the rhizome of Ligusticum chuanxiong Hort. (Chuanxiong). *Food Chem. Toxicol.* **2018**, *119*, 309–325. [CrossRef]
3. Feng, X.; Gong, Z.P.; Wang, L.J.; Yu, Y.T.; Liu, T.H.; Song, L.L. Behavior of maize particle penetrating a sieve hole based on the particle centroid in an air-screen cleaning unit. *Powder Technol.* **2021**, *385*, 501–516. [CrossRef]
4. Geng, R.H.; Yu, C.; Wang, Y.X.; Wang, X.W.; Zhang, X.K.; Li, R.L. Effect of external moisture content on screening performance of vibrating flip-flow screen and circular vibrating screen. *Minerals* **2023**, *13*, 16. [CrossRef]
5. Ma, Z.; Zhu, Y.L.; Wu, Z.P.; Traore, S.N.; Chen, D.; Xing, L.C. BP neural network model for material distribution prediction based on variable amplitude anti-blocking screening DEM simulations. *Int. J. Agric. Biol. Eng.* **2023**, *16*, 190–199. [CrossRef]
6. Wang, L.J.; Li, Y.H.; Wang, H.S.; Wang, B.; Ma, Z. Behavior of maize particles on the bionic sieve designed based on the earthworm's contour. *Powder Technol.* **2022**, *403*, 14. [CrossRef]
7. Shanmugam, B.K.; Vardhan, H.; Raj, M.G.; Kaza, M.; Sah, R.; Hanumanthappa, H. Investigation on the operational parameters of screening coal in the vibrating screen using Taguchi L27 technique. *Int. J. Coal Prep. Util.* **2022**, *42*, 3282–3291. [CrossRef]
8. Yuan, J.B.; Wang, J.F.; Li, H.; Qi, X.D.; Wang, Y.J.; Li, C. Optimization of the cylindrical sieves for separating threshed rice mixture using EDEM. *Int. J. Agric. Biol. Eng.* **2022**, *15*, 236–247. [CrossRef]
9. Ren, D.Z.; Yu, H.L.; Zhang, R.; Li, J.Q.; Zhao, Y.B.; Liu, F.B.; Zhang, J.H.; Wang, W. Research and experiments of hazelnut harvesting machine based on CFD-DEM analysis. *Agriculture* **2022**, *12*, 18. [CrossRef]
10. Li, X.P.; Zhao, G.Y.; Wang, W.Z.; Huang, Y.; Ji, J.T. Design and experiment of vibrating screen millet cleaning device with double-fan. *Appl. Eng. Agric.* **2021**, *37*, 319–331. [CrossRef]
11. Zhang, H.M.; Zhou, Z.; Qu, Z.; Li, Z.J.; Wang, W.Z. Simulation and experiment of sieving process of sieving device for tiger nut harvester. *Agriculture* **2022**, *12*, 16. [CrossRef]
12. He, D.Y.; Liu, C.S.; Li, S. The Nonlinear dynamic behavior of a particle on a vibrating screen based on the elastoplastic contact model. *Separations* **2022**, *9*, 14. [CrossRef]
13. Boriskina, Z.M.; Baryshnikova, O.O. The mathematical model of motion of particles in vibrating conveyors. *Int. J. Mech. Eng. Robot. Res.* **2020**, *9*, 76–79. [CrossRef]
14. Xin, L.L.; Liang, J.H. A dynamic analysis on the potato conveying and separation system considering the acting force of a material. *Trans. FAMENA* **2019**, *43*, 35–42. [CrossRef]
15. He, Y.M.; Liu, Q.; Lin, Y.; Zhang, X.L. Discussion on the transportation speed of the horizontally vibrating conveyor. In Proceedings of the International Conference on Advanced Engineering Materials and Technology (AEMT2011), Sanya, China, 29–31 July 2011; Trans. Tech. Publications Ltd.: Sanya, China, 2011; pp. 2497–2500. [CrossRef]
16. Zhang, Z.W.; Zhang, H.B.; Zhang, C. Study of material motion law in horizontal circling vibrating dryer. In Proceedings of the International Conference on Advanced Design and Manufacturing Engineering (ADME 2011), Guangzhou, China, 16–18 September 2011; Trans. Tech. Publications Ltd.: Guangzhou, China, 2011; pp. 2144–2147. [CrossRef]
17. Wang, L.J.; Ding, Z.J.; Meng, S.; Zhao, H.J.; Song, H.Q. Kinematics and dynamics of a particle on a non-simple harmonic vibrating screen. *Particuology* **2017**, *32*, 167–177. [CrossRef]
18. Han, I.; Lee, Y. Chaotic dynamics of repeated impacts in vibratory bowl feeders. *J. Sound. Vibr.* **2002**, *249*, 529–541. [CrossRef]
19. Ma, Z.; Han, M.; Li, Y.M.; Gao, H.Y.; Lu, E.; Chandio, F.A.; Ma, K.C. Motion of cereal particles on variable-amplitude sieve as determined by high-speed image analysis. *Comput. Electron. Agric.* **2020**, *174*, 9. [CrossRef]
20. Song, G.Z.; Huang, F.G.; Pan, J.F. Feasibility analysis of calcium carbonate particle trajectory simulation in a dual horizontal shaft mixer. *Materials* **2023**, *16*, 16. [CrossRef] [PubMed]
21. Yang, H.R.; Ma, X.D. Research on the screening mechanisms of composite vibrating screens based on discrete elements. *PLoS ONE* **2023**, *18*, 19. [CrossRef]
22. Maul, G.P.; Thomas, M.B. A systems model and simulation of the vibratory bowl feeder. *J. Manuf. Syst.* **1997**, *16*, 309–314. [CrossRef]
23. Zhou, S.; Zhang, G.G.; Xu, X.Y. Experimental study on the velocity of bed load movement based on high-speed imaging technology J. *J. Sediment Res.* **2023**, *48*, 8–13. [CrossRef]
24. Sun, H.; Chen, Z.M. *Theory of Machines and Mechanisms*, 7th ed.; Higher Education Press: Beijing, China, 2006; pp. 11–73.
25. Tian, L.; Cao, C.M.; Zhang, Y.; Qing, K.; Ge, J.; Fang, L.F. Design and experiment of combine Radix peucedani harvester. *J. Anhui Agric. Univ.* **2022**, *49*, 815–822. [CrossRef]
26. Dai, F.; Song, X.F.; Zhao, W.Y.; Zang, F.W.; Ma, H.J.; Ma, M.Y. Simulative calibration on contact parameters of discrete elements for covering soil on whole plastic film mulching on double ridges. *Trans. Chin. Soc. Agric. Eng.* **2019**, *50*, 49–56. [CrossRef]
27. Kong, X.X.; Xing, J.X.; Wen, B.C. Analysis of motion of the part on the linear vibratory conveyor. *J. Northeast. Univ. Nat. Sci.* **2015**, *36*, 827–831. [CrossRef]
28. Xu, S. Research on Calculation Method of Falling Rock Impact Force. Master's Thesis, Chongqing Jiaotong University, Chongqing, China, 2016.
29. Ding, W.S.; Tian, L.; Liu, K. Analysis of transient impact dynamic characteristics of hydraulic impact hammer. *J. South. China Univ. Technol.* **2016**, *44*, 63–70. [CrossRef]

30. Li, Z.F.; Liang, J.B.; Jia, P.Y.; Zheng, S.Q.; Zhou, H.Z.; Tong, X. Segmented research and parameter optimization of double-layer vibrating screen. *Eng. Comput.* **2023**, *40*, 852–867. [CrossRef]
31. Shen, G.L.; Chen, Z.Q.; Wu, X.Q.; Li, Z.F.; Tong, X. Stepwise shape optimization of the surface of a vibrating screen. *Particuology* **2021**, *58*, 26–34. [CrossRef]
32. Yan, D.X.; Xu, T.Y.; Yu, J.Q.; Wang, Y.; Guan, W.; Tian, Y.; Zhang, N. Test and Simulation Analysis of the Working Process of Soybean Seeding Monomer. *Agriculture* **2022**, *12*, 14. [CrossRef]
33. Yang, Q.Z.; Zhang, R.Y.; Jia, C.P.; Li, Z.Y.; Zhu, M.L.; Addy, M. Study of dynamic hole-forming performance of a cup-hanging planter on a high-speed seedling transplanter. *Front. Mech. Eng.* **2022**, *8*, 16. [CrossRef]
34. Tong, Z.W. Design and Experiment of Compound Cutting Parts of Tobacco Hilling Machine. Master's Thesis, Henan Agricultural University, Zhengzhou, China, 2020.